Self-broadening of the sodium resonance lines and excitation transfer between the $3P_{3/2}$ and $3P_{1/2}$ levels

J. Huennekens* and A. Gallagher†
Joint Institute for Laboratory Astrophysics, University of Colorado and National Bureau of Standards, Boulder, Colorado 80309
(Received 4 October 1982)

Sodium vapor, in the density range 10^{13} to 5×10^{14} cm^{-3}, was excited by a cw dye laser, tuned 20–150 GHz from either the D_1 or D_2 resonance line. We observed a three-peak scattered spectrum, consisting of the Rayleigh component at the laser frequency, and the two fluorescence components (direct and sensitized) at the atomic resonance-line frequencies. Corrections to the Rayleigh signals for anisotropy and polarization effects, and to the fluorescence signals for radiation trapping, were made in order to obtain the ratio of the sum of the total intensities of the two fluorescence components to that of the Rayleigh component. This ratio combined with a measurement of the line-wing absorption coefficient yields the sodium density and the D-line self-broadening rate coefficients [$k_{br}=4.67\times10^{-7}$ cm^{3}s^{-1} ($\pm15\%$) for the D_2 line and $k_{br}=3.07\times10^{-7}$ cm^{3}s^{-1} ($\pm15\%$) for the D_1 line]. Asymmetry in the self-broadened line wings due to fine-structure recoupling was observed. The measured intensity ratio of the D lines, combined with pulsed measurements of the effective radiative decay rates in the presence of radiation trapping, yields the fine-structure collisional-mixing cross section [$\sigma(3P_{3/2}\rightarrow3P_{1/2})=172$ Å^2 ($\pm18\%$)] at $T\cong300°$ C. Our results are compared to other experiments and to theory.

I. INTRODUCTION

The interaction between excited ($3P$) and ground-state ($3S$) sodium atoms is an extremely strong long-range interaction which should be well characterized by the resonant dipole-dipole interaction. The collisional broadening of the $3S$-$3P$ resonance line and the $3P_{3/2}\leftrightarrow3P_{1/2}$ excitation-transfer process both result from this supposedly well-characterized interaction, so that accurate calculations of these cross sections should be possible. However, two previous measurements[1,2] of the excitation-transfer cross section are subject to significant uncertainties and are in considerable disagreement, while the only resonance-line broadening measurement[3] barely agrees with theory[4,5] within rather large experimental uncertainties. The present measurements are directed toward improving the accuracy of both measurements. Our most important improvement has been an independent measurement of the perturber (Na atom) density responsible for both processes.

Measurements of resonance broadening and depolarization are complicated by the high optical depths necessary to obtain significant broadening. In the past, high resonance-line optical depths have been circumvented by observing transitions whose lower level is the resonance state,[6–9] by using isotopic mixtures,[10,11] by observing branching transitions,[12] and by measuring absorption coefficients in the line wings.[3,13,14] The present experiment uses a different method, described below, based on the spectral separation of Rayleigh and fluorescence light. All of these methods require knowledge of the vapor density, and in the experiments involving metal atoms, large uncertainties are generally introduced if densities are taken from vapor pressure versus temperature relationships. Thus, as noted above, we have here independently measured the vapor pressure.

The theory of resonance broadening has advanced steadily since Holtsmark's[15] pioneering work, especially for $J=0$ to 1 transitions where good (~5–10%) agreement between the available experimental results and theory has now been obtained in the impact region.[16] Ali and Griem[4] and Carrington, Stacey, and Cooper[5] have extended the calculations to include $J=\frac{1}{2}$ to $J=\frac{1}{2}$ and $J=\frac{1}{2}$ to $J=\frac{3}{2}$ transitions relevant to the alkali-metals, but without the inclusion of the fine-structure recoupling described by Movre and Pichler,[17] which has a major effect in the line wings. The resonance-broadening measurements carried out in absorption by Niemax and Pichler[3] on sodium, potassium, rubidium, and cesium yield broadening rate coefficients k_{br} that barely agree within 50% uncertainties with the calculations, although the more recent results of Niemax, Movre, and Pichler[14] in rubidium and cesi-

um are in good agreement with the calculations but are uncertain by $\sim 30\%$. Lewis *et al.*[9] obtained $k_{\rm br}$ in potassium that differ by $\sim 30\%$ from the Carrington *et al.* calculations and are uncertain by the same amount.

In our measurements of the sodium D_1 and D_2 resonance-broadening rates, we have circumvented optical-depth problems by tuning a cw laser (frequency ω_L) slightly off resonance and observing the ratio $R(\omega_L)$ of the collisionally redistributed fluorescence at the atomic frequencies ω_1 and ω_2 to the nonredistributed Rayleigh scattered light at the laser frequency ω_L. One advantage of this method is that we were able to accurately measure $k_{\rm br}$ at very low densities where the collisional width is smaller than the natural width; this would be very difficult in an absorption experiment. But the crucial advantage is that we can combine measurements of $R(\omega_L)$ with line-wing absorption measurements to yield both the resonance-broadening parameter and the vapor density, thus eliminating the major source of uncertainty in these alkali-metal broadening measurements.

We have also measured the ratio of the sensitized to direct fluorescence and the resonance-line radiation decay rates in the presence of radiation trapping. From these data we obtain cross sections for excitation transfer between the $3P_{3/2}$ and $3P_{1/2}$ fine-structure levels due to collisions with ground-state sodium atoms. These processes are described by

$$\mathrm{Na}(3P_{3/2})+\mathrm{Na}(3S)\underset{\sigma_{12}}{\overset{\sigma_{21}}{\rightleftarrows}}\mathrm{Na}(3P_{1/2})+\mathrm{Na}(3S)\ . \tag{1}$$

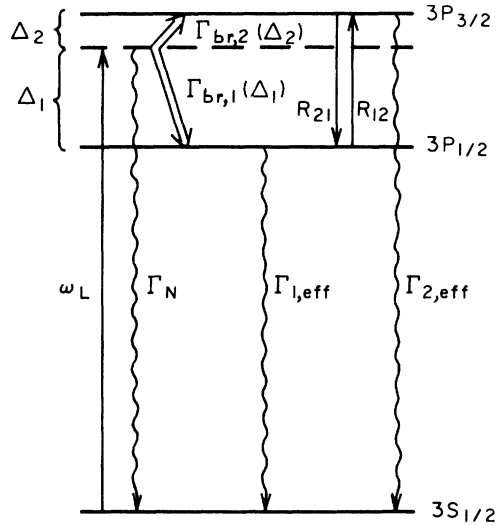

FIG. 1. Collisional and radiative rates for laser excitation near the sodium D lines. See text for explanations of terms.

II. MODEL

Figure 1 shows the relevant collisional and radiative rates which occur in sodium excited near the D lines. R_{21} and R_{12} are the excitation-transfer rates between the $3P_{3/2}$ and $3P_{1/2}$ levels due to collisions with ground-state atoms. $\Gamma_{\rm br,1}(\Delta_1)$ and $\Gamma_{\rm br,2}(\Delta_2)$ are the total collisional-transfer rates from the "virtual" level to the $3P_{1/2}$ and $3P_{3/2}$ levels, respectively. Here $\Delta_1 \equiv \omega_L - \omega_1$ and $\Delta_2 \equiv \omega_L - \omega_2$. For arbitrary ω_L, $\Gamma_{\rm br1}(\Delta_1)$ and $\Gamma_{\rm br,2}(\Delta_2)$ each involve the full set of states that separate to the $3P_{1/2}$ and $3P_{3/2}$ levels. [This is in contrast to the case of well-isolated states where only the $3P_{3/2}$ levels would affect $\Gamma_{\rm br,2}(\Delta_2)$.] These collisional rates are further complicated by the fact that the virtual level is a coherent superposition of the ground state and both excited states. However, for $\Delta_2 \ll 1/\tau_c \ll \Delta_1$, where τ_c is the duration of a collision, the term $\Gamma_{\rm br,2}(\Delta_2)$ reduces to a constant $\Gamma_{\rm br,2} \equiv n k_{\rm br,2}$, which is the desired impact-regime self-broadened linewidth [full width at half maximum (FWHM)] of the D_2 line. ($\Gamma_{\rm br,2}$ can then be thought of as the collisional rate of destruction of optical coherence.) In this limit, $\Gamma_{\rm br,1}(\Delta_1)$ approaches the inelastic rate R_{21}. [This has been derived in a dressed-level analysis, where at low fields the transition rate between the dressed states is $(\Omega^2/4\Delta_2^2)R_{21}$. The term $\Omega^2/4\Delta_2^2$, where Ω is the Rabi frequency, corresponds to absorption to the virtual level in the bare-atom picture (see Ref. 18).] $\Gamma_{\rm br,1}(\Delta_1)$ can then be ignored at the densities used here since radiation trapping causes this term to be a negligible source of $3P_{1/2}$ population compared to the subsequent $3P_{3/2} \rightarrow 3P_{1/2}$ excitation transfer that occurs during the slow decay of the excited-state population. Similarly, for $\Delta_1 \ll 1/\tau_c \ll \Delta_2$ the term $\Gamma_{\rm br,1}(\Delta_1)$ reduces to a constant $\Gamma_{\rm br,1} \equiv n k_{\rm br,1}$ and $\Gamma_{\rm br,2}(\Delta_2)$ tends towards R_{12} and can also be ignored.[19] The other Γ's in Fig. 1 are radiative rates. It must be noted that while the off-resonant Rayleigh scattering at ω_L is characterized by the natural radiative rate Γ_N, the two fluorescence components decay at the much slower effective rates $\Gamma_{1,\rm eff}$ and $\Gamma_{2,\rm eff}$ due to radiation trapping at the high optical depths in our cell.

The simple model indicated by the figure yields the following expression for $R(\Delta_2)$, the sum of the fluoresence intensities divided by the Rayleigh intensity, for the laser tuned near the D_2 line ($\Delta\nu_{\rm Doppler} \ll \Delta_2 \ll 1/\tau_c \ll \Delta_1$):

$$R(\Delta_2) \equiv \frac{I_{D_1}+I_{D_2}}{I_{\rm Rayleigh}} = \frac{\Gamma_{\rm br,2}}{\Gamma_N}\ . \tag{2}$$

Equation (2), which is also valid with 2 replaced by 1 for detunings near the D_1 line, has been derived[18]

more rigorously in the weak-field limit using a rate-equation approach in "dressed levels."[20,21] When $\Gamma_{\rm tot} \equiv \Gamma_N + \Gamma_{\rm br} \ll \Delta_2 \ll 1/\tau_c$, the absorption coefficient $k_\nu(\Delta_2)$ for $\Delta\nu_{\rm Doppler} \ll \Delta_2 \ll 1/\tau_c \ll \Delta_1$ can be written as

$$k_\nu(\Delta_2) = \frac{\Gamma_N + \Gamma_{\rm br}}{(\Delta_2)^2} Kn \ , \tag{3}$$

where $K = (\lambda^2/8\pi)(g^*/g)\Gamma_N$ is known. Here g^* and g are the upper- and lower-state statistical weights and n is the Na density. Consistent with Eq. (2), the Γ_N part of k_ν yields Rayleigh scattering at ω_L, while the $\Gamma_{\rm br}$ part yields the fluorescence or redistributed components at ω_2 and ω_1.

Similarly, an analysis using the rate-equation approach of Fig. 1 (or a more formally correct dressed-atom approach) yields the following D_1 to D_2 fluorescence ratio for excitation near D_2:

$$\frac{I_{D_1}}{I_{D_2}} \cong \frac{R_{21}\Gamma_{1,\rm eff}(\Gamma_{\rm br,2} + \Gamma_{2,\rm eff})}{\Gamma_{2,\rm eff}\Gamma_{\rm br,2}(\Gamma_{1,\rm eff} + R_{12})} \ . \tag{4}$$

At densities above 5×10^{13} cm^{-3}, $\Gamma_{2,\rm eff} < 1.5\times10^5$ s^{-1} as measured in our geometry (see Sec. VII and Refs. 18 and 22) and $\Gamma_{\rm br,2} > 2.2\times10^7$ s^{-1} (see Table I). In this limit Eq. (4) becomes

$$\frac{I_{D_1}}{I_{D_2}} \cong \frac{R_{21}\Gamma_{1,\rm eff}}{\Gamma_{2,\rm eff}(\Gamma_{1,\rm eff} + R_{12})} \ . \tag{5}$$

Expression (5) is intuitively obvious since $R_{21}/\Gamma_{2,\rm eff}$ is the probability that an atom in the $3P_{3/2}$ state undergoes a transfer collision before it can emit a D_2 photon that escapes the cell, and $\Gamma_{1,\rm eff}/(\Gamma_{1,\rm eff} + R_{12})$ is the probability that the collisionally populated $3P_{1/2}$ level will decay by radiating a D_1 photon that escapes the cell. From Eq. (4) we obtain for the laser tuned near the D_2 line

$$R_{21} = \frac{\Gamma_{1,\rm eff} I_{D_1}/I_{D_2}}{\beta_2(\Gamma_{1,\rm eff}/\Gamma_{2,\rm eff}) - \alpha(I_{D_1}/I_{D_2})} \ . \tag{6a}$$

Similarly, we obtain

$$R_{21} = \frac{\Gamma_{2,\rm eff} I_{D_2}/I_{D_1}}{\alpha\beta_1(\Gamma_{2,\rm eff}/\Gamma_{1,\rm eff}) - (I_{D_2}/I_{D_1})} \tag{6b}$$

for the laser tuned near D_1. In these expressions β_i is defined as $\beta_i \equiv (\Gamma_{{\rm br},i} + \Gamma_{i,\rm eff})/\Gamma_{{\rm br},i}$ and α is defined as $\alpha \equiv R_{12}/R_{21}$, which equals 1.91 at $T = 300$ °C.

III. EXPERIMENT

Figure 2 is a block diagram of the experimental arrangement. The sodium cell is a 5-cm stainless-steel block drilled out to make a cross. Sapphire windows were vacuum sealed to the block with metal O rings. Details of the cell construction may be found in Refs. 18 and 22. As indicated, two arms of the hollow cross contain sapphire rods which reduce the optical depth in the detection direction. The sodium density is controlled by the temperature of a sidearm which is typically 30 °C below the cell temperature. The sodium density was measured at $\sim10^{12}$ cm^{-3} (using photomultiplier PMT2 in the figure) by measurement of k_0, the Doppler-broadened line-center absorption coefficient ($k_0/n = 6.2\times10^{-12}$ cm^2 for the D_2 line at $T = 420$ K). At $\sim10^{14}$ cm^{-13}, the density was obtained by measuring both the wing absorption coefficient k_ν, and the ratio of the fluorescence to Rayleigh signal $\Gamma_{\rm br}/\Gamma_n$. Using Eq. (2) in Eq. (3) it can be seen that the Na density is given in this case by

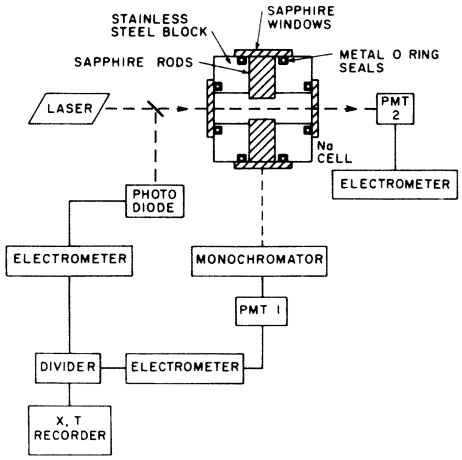

FIG. 2. Block diagram of experimental setup. Cross section of the cell is shown; Na is confined to the cross bored through the stainless-steel block but is excluded from the two arms containing sapphire rods (indicated by cross hatching). Stainless-steel block is directly heated and sits inside an insulating firebrick oven with brass liner and quartz windows which minimizes cooling of the cell's sapphire windows. PMT is a photomultiplier in the figure.

$$n = \Delta_2^2 k_\nu(\Delta_2)/\{K\Gamma_N[1 + R(\Delta_2)]\} \ . \tag{7}$$

[In Sec. IV we will show that Eq. (2) must be modified as in Eq. (8) and $R(\Delta_2)$ above must be replaced by $R_{\rm meas}F_{\rm Rayleigh}(\theta,\phi)/CF_{\rm fl}(\theta,\phi)$.] Therefore n can be found from the measured quantities $\Delta_2, k_\nu(\Delta_2)$, and $R(\Delta_2)$. The two quantities $\Delta_2^2 k_\nu(\Delta_2)$ and $R(\Delta_2)$ are independent of Δ_2 in this approximation and need not be measured at the same detuning. In fact, they both vary slowly with Δ_2 and the limit of each as $\Delta_2 \to 0$ is used in Eq. (7). Vapor pressures obtained in this manner were 2—13% above Nesmeyanov's[23] relationships.

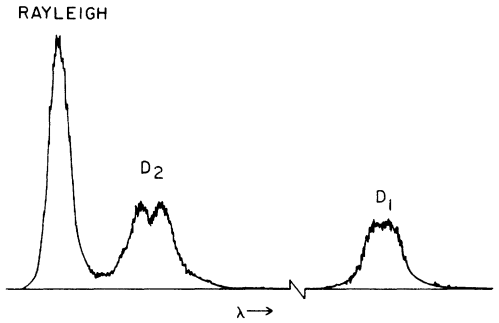

FIG. 3. Spectrometer scan of Rayleigh, D_2, and D_1 components. Laser was detuned ~ 31 GHz to the red of D_2. Na density equals 1.51×10^{14} cm^{-3}. Note self-reversal on the D_2 fluorescence component due to radiation trapping.

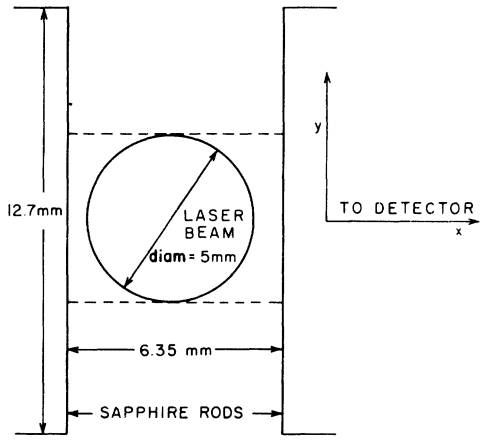

FIG. 4. Cross section of the cell. Laser beam propagates into the page (in along the z axis). Light is detected perpendicular to the sapphire-rod surface (in the x direction). Spectrometer collects light entering a slit oriented along y. The region between the dashed lines is observed in the excitation-transfer experiment and in the line-shape studies. For absolute $k_{\rm br}$ determinations, the fluorescence to Rayleigh ratio was measured over the entire y dimension of the sapphire-rod surface.

The laser is a single-mode cw dye laser with an ~ 1-MHz linewidth. The detunings of 20—150 GHz were determined by setting the laser frequency on either the $F=2$ component of each resonance line or on the $(F=2)$-$(F=1)$ crossover resonance, observed with a saturated absorption cell (see Ref. 18), and then "hopping" thick etalon modes by tilting the laser thin etalon. In this way, we were able to fix detunings in multiples of 9.95-GHz steps.

The scattered spectrum was collected at 90° to the laser beam with a $\frac{3}{4}$-double monochromator and a photomultiplier with an S-20 cathode response. Figure 3 shows a typical spectrometer scan; note the self-reversal apparent on the D_2 fluorescence peak due to radiation trapping at the high optical depths used.

IV. CORRECTION FACTORS

The intensities appearing in Eq. (2) are the total intensities, summed over polarization and integrated over angle. Since we only detect light in a single direction θ,ϕ and since both the Rayleigh and fluorescence light emerge from the cell anisotropically, the intensities in Eq. (2) must be multiplied by anisotropy correction factors $F_{\rm Rayleigh}$ and $F_{\rm fl}$ to yield the detected fluorescence to Rayleigh ratio. Radiation trapping is the cause of the fluorescence anisotropy, while the Rayleigh scattering is polarized and therefore anisotropic near the D_2 line but unpolarized and isotropic near D_1. Additionally, since the Rayleigh scattered light near D_2 that escapes the cell is partially polarized and our detection system is not equally sensitive to both polarizations, the detected intensities must be corrected for this effect. This is discussed in Ref. 18 and will not be discussed further here, except to note that the magnitude of this correction was $<11\%$, and it introduced minor uncertainty into the final result. The large number of trapping events undergone by fluorescence photons completely depolarizes the fluorescence signals.

The Rayleigh scattering occurs in the laser-excited region, whereas the fluorescence comes from a more extended region due to radiation diffusion. A portion of the fluorescence is not detected due to the finite vertical extent of the windows (see Fig. 4) so we introduce a correction factor C to account for this. Putting these correction factors into Eq. (2) yields for the laser tuned near the D_2 line

$$R_{\rm meas}\equiv\left.\frac{I_{D_2}+I_{D_1}}{I_{\rm Rayleigh}}(\theta,\phi)\right|_{\rm measured}$$

$$=\frac{\Gamma_{{\rm br},2}}{\Gamma_N}\frac{F_{\rm fl}(\theta,\phi)C}{F_{\rm Rayleigh}(\theta,\phi)}\ . \tag{8}$$

It can be shown that, for Δ_1 and Δ_2 large compared to the Doppler and hyperfine structure widths, the Rayleigh intensity emitted at an angle θ to the direction $\hat{z}$ of the laser E field with polarization perpendicular to $\hat{z}$ or with a component parallel to $\hat{z}$ is given by[24–26]

$$I_{\rm Rayleigh}(\epsilon_\perp,\theta)\propto\left|\frac{1}{\Delta_1}-\frac{1}{\Delta_2}\right|^2 \tag{9a}$$

and

$$I_{\text{Rayleigh}}(\epsilon_{||},\theta) \propto \left| \frac{1}{\Delta_1} + \frac{2}{\Delta_2} \right|^2 \sin^2\theta + \left| \frac{1}{\Delta_1} - \frac{1}{\Delta_2} \right|^2 \cos^2\theta \,. \quad (9b)$$

For $\theta = 90°$, these results reduce to those given by Tam and Au[27] for that geometry. Our sapphire rod and window partially scramble polarization, so that we measure a total Rayleigh intensity $I_{\text{Rayleigh}}(\theta) = I_{\text{Rayleigh}}(\epsilon_1,\theta) + I_{\text{Rayleigh}}(\epsilon_{||},\theta)$ given by

$$I_{\text{Rayleigh}}(\theta) \propto \frac{2}{\Delta_1^2} + \frac{2+3\sin^2\theta}{\Delta_2^2} + \frac{6\sin^2\theta - 4}{\Delta_1\Delta_2} \,. \quad (10)$$

We have shown[18] that Eq. (10) yields

$$F_{\text{Rayleigh}} \cong \tfrac{1}{2} + \tfrac{3}{4}\sin^2\theta \quad (11a)$$

for ω_L near ω_2 and

$$F_{\text{Rayleigh}} \cong 1 \quad (11b)$$

for ω_L near ω_1. Owing to the orientation of our entrance sapphire window, linearly polarized light at $\theta = 56°$ and 146° was used and the relative intensities of Rayleigh scattering for $\theta = 56°$ and 146° were measured as a function of Δ_1 and Δ_2. The measurements agree with Eq. (10) to within the statistical measurement uncertainty.

The fluorescence anisotropy results from the attenuation of resonance radiation with distance, due to trapping. Fluorescence photons emitted in a direction normal to the sapphire-rod face (which are those that we detect) travel through the minimum column length of sodium atoms (see Fig. 4) and therefore have a higher probability of escape. Such emission is thus enhanced relative to an isotropic distribution. The escape anisotropy is symmetric for both rods since the excited-atom distribution is symmetric about $x = L/2$, where L is the rod spacing. The emission anisotropy out each rod is essentially the same for all atoms that are more than a few optical depths from the rod surface, and nearly all the emission comes from such atoms since the excited atoms are distributed in the x direction in nearly an infinite-slab fundamental-mode distribution.[28] Thus we have calculated[18] the escape anisotropy using Holstein's probabilities $P(l)$ of fluorescence transmission through a distance l of vapor, i.e., $P(l) \simeq (k_0 l)^{-1}[\pi \ln(k_0 l)]^{-1/2}$ in the density range where trapping is dominated by Doppler broadening, and $P(l) \simeq (\pi k_p l)^{-1/2}$, where $k_p = (\lambda^2/2\pi) n (g^*/g)(\Gamma_N/\Gamma_{\text{br}})$, in the range where trapping is dominated by impact broadening.[28] The result for both D lines, averaged over a symmetric excited-atom distribution between the windows, is $F_{\text{fl}} \cong 2$ for the Doppler case ($n < 6\times10^{13}$ cm^{-3}) and $F_{\text{fl}} = 1.5$ for the impact case ($n > 1\times10^{14}$ cm^{-3}). (See Ref. 22 for experimental verification of the validity of Holstein's theory at these densities.)

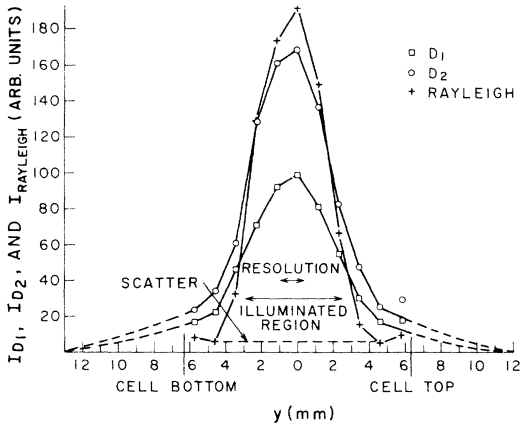

FIG. 5. Signal intensities vs vertical position y (see Fig. 4). □'s are D_1 fluorescence, ○'s are D_2 fluorescence, and + 's are Rayleigh scattering. [Na] $= 1.97\times10^{14}$ cm^{-3} and the laser was tuned ~41 GHz to the red of the D_2 line. Position resolution was 1 mm. Beam diameter was 5 mm. $\theta = 56°$ [see Eq. (10)]. Dashed lines represent extrapolations beyond the sapphire-rod edges.

Comparisons made with a detailed computer calculation,[29] which used Voigt line shapes and a more sophisticated radiation transfer theory and considers all atoms in the vessel as well as motion of the absorbers and wall quenching, indicate that these results should be accurate to within a few percent for our experimental conditions.

To obtain the value of the correction factor C, we have measured the fluorescence and Rayleigh intensities as a function of the y position along the sapphire-rod surface (see Fig. 4). Signals are expected to be independent of z due to symmetry in that direction. Figure 5 is a plot of the intensities of each of the three spectral components as a function of y for $n = 1.97\times10^{14}$ cm^{-3}. Some D-line fluorescence escapes to the cell walls beyond the top and bottom window edges, and the intensity of this undetected light should be added to the detected fluorescence signals to be consistent with our infinite-slab approximation in evaluating F_{fl}. The extrapolated dashed lines in Fig. 5 are estimates of this undetected fluorescence. The areas under the curves within the window region divided by the areas under the corresponding complete curves, in-

TABLE I. Determination of $k_{br,2}$ and $k_{br,1}$.

Density (cm^{-3})	Line pumped	$\frac{I_{D_2}+I_{D_1}}{I_{Rayleigh}}$	$F_{Rayleigh}$	F_{fl}	C	Γ_{br}[a] ($10^7\ s^{-1}$)	k_{br}[b] ($10^{-7}\ cm^3/s$)
1.97×10^{14}	D_2	1.89[c]	1.02	1.50	0.901	9.00	4.57
1.97×10^{14}	D_2	1.99[d]	1.02	1.50	0.901	9.47	4.81
3.25×10^{13}	D_2	0.390[c]	1.02	2.00	0.855	1.47	4.51
3.08×10^{13}	D_2	0.543[d]	0.735	2.00	0.855	1.47	4.77
1.97×10^{14}	D_1	1.26[c]	1.00	1.50	0.901	5.86	2.97
3.08×10^{13}	D_1	0.265[c]	1.00	2.00	0.855	9.73	3.16

[a] $\Gamma_{br}=\Gamma_N[(I_{D_2}+I_{D_1})/I_{Rayleigh}][F_{Rayleigh}/(F_{fl}C)]$ from Eq. (8).

[b] $k_{br}=\Gamma_{br}/n$.

[c] Fluorescence to Rayleigh ratio obtained by observing over full 12.7-mm y dimension of the sapphire rods.

[d] Fluorescence to Rayleigh ratio obtained by integrating the 1-mm resolution signals plotted as in Fig. 5 over the full y dimension of the sapphire rods.

cluding the extrapolations, yield the correction ratios C. These determinations of C, listed in Table I, were made at the same densities that were used for the absolute measurements of k_{br}. At [Na] $=3.08\times10^{13}\ cm^{-3}$ we found $C=0.855$, while at [Na] $=1.97\times10^{14}\ cm^{-3}$, $C=0.90$.

An approximate calculation of the expected y distribution of excited atoms using Holstein's escape probabilities $P(l)$ can also be used to obtain a lower bound on the factor C. We have shown[18] that $n_e(y)$ falls off at least as fast as $y^{-5/2}$ which yields $C_{min}=0.83$ when combined with data such as that in Fig. 5. Since this is a lower bound, we believe our extrapolations that yielded 0.855 and 0.90, respectively, are better estimates. We estimate that the uncertainty in C is $\sim8\%$ at the lower density and $\sim5\%$ at the higher density (i.e., half of the magnitude of the correction).

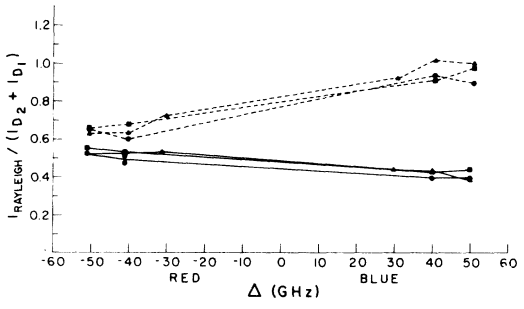

FIG. 6. Measured ratio of the total Rayleigh intensity to the sum of the two fluorescence component intensities with detection over the full y dimension of the sapphire-rod surface. Detunings are with respect to the D_1- and D_2-line centroids. Different lines represent different data runs. Solid lines are pumping D_2, dashed lines are pumping D_1. [Na] $=1.97\times10^{14}\ cm^{-3}$. Note $\theta=56°$ [see Eq. (10)].

V. RESULTS FOR k_{br}

Using the Na densities obtained as described in Sec. III and Eq. (7), we can use Eq. (8) to yield the resonance-broadening parameters $k_{br,1}\equiv\Gamma_{br,1}/n$ and $k_{br,2}\equiv\Gamma_{br,2}/n$. The data reductions are given in Table I. The intensity ratios marked with a c in the table came from measurements where we imaged the full y height of the window (the full 12.7-mm region in Fig. 4). In these cases, we used several detunings, both positive and negative, and then we interpolated the signals to zero detuning (see Fig. 6). Those intensity ratios marked by a d were obtained by measuring all intensities as a function of y, as in Fig. 5, integrating over y, and then interpolating to zero detuning. These fluorescence to Rayleigh ratios are slightly higher than those marked c. We believe this discrepancy is due to the more accurate correction of the d-marked intensities for the small amount of Rayleigh light scattered off walls (note that the Rayleigh points at ±6 mm in Fig. 5 are anomalously high).

Relative measurements of the intensity ratio as a function of sodium density show the expected linear density dependence of Γ_{br} (see Ref. 18).

From Table I, we arrive at the following average values for $k_{br,1}$ and $k_{br,2}$ (of $\pm15\%$ accuracy):

$$k_{br,2}=4.67\times10^{-7}\ cm^3s^{-1}\ , \tag{12a}$$

$$k_{br,1}=3.07\times10^{-7}\ cm^3s^{-1}\ , \tag{12b}$$

where the listed uncertainties were obtained as discussed below.

The uncertainty in $F_{Rayleigh}$ should be negligible since the theoretical calculation of Sec. IV is on a

sound footing and should be limited only by window and polarizer imperfections. Our approximation of ignoring hyperfine structure is valid since the laser detuning is large compared to all hyperfine splittings.

For the densities used, we expect F_{fl} to be accurate to $\sim 5\%$ at the higher density and to $\sim 10\%$ at the lower density, where we neglected the log term in the Holstein-theory Doppler-case escape probability. These uncertainties also include a minor systematic uncertainty associated with the fact that F_{fl} decreases near the top and bottom of the cell due to a breakdown of the infinite-slab approximation. This small systematic error is in the direction of causing our reported values to be too low.

As mentioned in Sec. IV, we estimate the uncertainty in the factor C is less than 5% at the higher density and less than 8% at the lower density. We estimate the statistical uncertainty of the data at $\sim 5\%$.

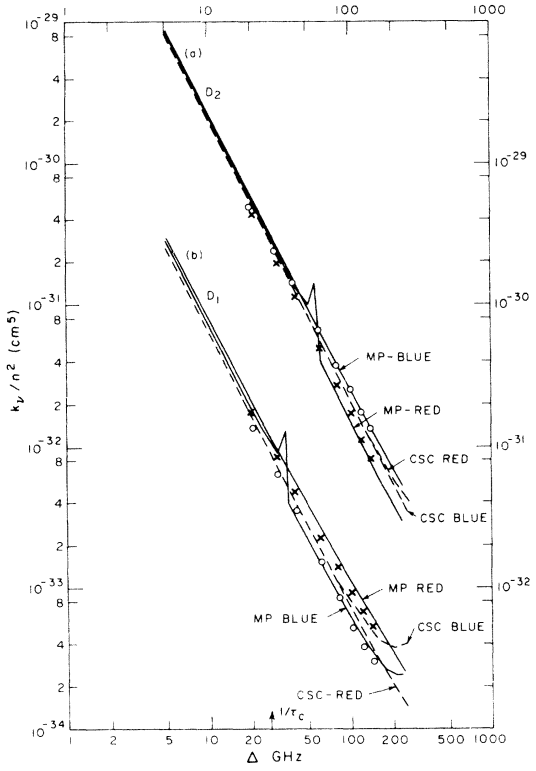

FIG. 7. k_ν/n^2 vs detuning for the sodium D_1 and D_2 lines. Solid lines are quasistatic calculations of Movre and Pichler (Ref. 17). Dashed lines are impact-regime calculations of Carrington *et al.* (Ref. 5), where we have added the contributions of the two fine-structure levels incoherently. O's are present experimental results taken with detunings to the blue of the respective lines. x's are results for detunings to the red of the respective lines. $[\mathrm{Na}]=1.51\times 10^{14}$ cm^{-3}. Arrow indicates the approximate value of $1/\tau_c$ for self-broadening of the sodium D lines.

Figure 6 shows measured Rayleigh to fluorescence ratios as a function of detuning. As can be seen, our interpolations to zero detuning assume a linear asymmetry. We estimate that this linear interpolation for obtaining the impact-regime limit of k_{br} introduces a maximum uncertainty of a few percent (see Ref. 18).

We believe the uncertainty in our knowledge of the sodium density is approximately 10% (see Ref. 18).

Other sources of error are small or care was taken to avoid them. Scattered light contributed a few percent to the Rayleigh signal, but we corrected for this. The F_{fl} calculation ignored the dependence of the sapphire reflectivity on angle; estimates of this led to $\sim 1\%$ correction. The program, "SLAB 3,"[29] demonstrates that the destruction of excited atoms by wall quenching is less than a 2% effect at the highest density we used, where it is expected to be most significant. Theoretical and experimental checks were made to assure that optical-pumping effects were not important at our laser powers (~ 10 mW) and detunings (>20 GHz). A calculation of Na_2 concentrations[30,31] was carried out and indicates $[Na_2]<10^{12}$ cm^{-3} at our highest density. This is below 1% of the atomic sodium density, and from the molecular rate coefficients measured by Lam *et al.*[31] we believe no molecular collision process is of importance to our results.

Assuming that no correlations among the systematic errors exist, we combined the above uncertainties in quadrature. Thus we assign an overall uncertainty of $\pm 15\%$ to the average values obtained in Table I and listed in Eq. (12).

VI. SELF-BROADENED LINE SHAPE

In the impact regime ($\Delta\omega \ll 1/\tau_c$, where τ_c is the duration of a collision), but well outside the hyperfine structure and Doppler widths, the absorption coefficient k_ν is given by[32,33]

$$k_\nu(\text{impact})=\frac{\lambda^2}{8\pi}\frac{g^*}{g}\Gamma_N\frac{n\Gamma}{(\Delta\omega)^2+(\Gamma/2)^2}\ , \qquad (13)$$

where λ is the transition wavelength, and Γ is the total width (FWHM) of the line.

In the opposite limit ($\Delta\omega \gg 1/\tau_c$) or the quasistatic regime, the absorption coefficient is given by[3,34,35]

$$k_\nu(\text{quasistatic})=\frac{\lambda^2}{8\pi}\frac{g^*}{g}\Gamma_N\left[\frac{\pi^2 C_3 n^2}{(\Delta\omega)^2}\right] \qquad (14)$$

assuming an interaction of the form $\Delta\omega=C_3/R^3$.

TABLE II. Determination of σ_{21} and σ_{12}.

Density (10^{13} cm^{-3})	I_{D_1}/I_{D_2}	$\Gamma_{1,\text{eff}}$[a] (10^5 s^{-1})	$\Gamma_{2,\text{eff}}$[a] (10^5 s^{-1})	α[b]	β_2[c] or β_1[c]	$\bar{v}$[d] (10^5 cm/s)	R_{21}[e] (10^4 s^{-1})	k_{21}[f] (10^{-9} cm^3/s)	σ_{21}[g] (Å^2)	σ_{12}[h] (Å^2)
					Pump D_2					
6.86	0.499	2.42	1.33	1.92	1.004	1.036	13.9	2.03	196	376
5.33	0.366	3.22	1.57	1.92	1.006	1.036	8.29	1.56	150	288
3.28	0.198	5.50	2.58	1.91	1.016	1.022	6.09	1.86	182	347
3.25	0.194	5.52	2.60	1.92	1.017	1.033	5.99	1.84	179	343
3.08	0.185	5.90	2.78	1.92	1.019	1.034	6.04	1.96	190	364
2.75	0.141	6.75	3.12	1.91	1.024	1.021	4.89	1.78	174	333
2.07	0.0838	9.30	4.30	1.91	1.043	1.021	3.72	1.80	176	336
					Pump D_1					
6.86	0.497	2.42	1.33	1.92	1.012	1.036	11.4	1.66	160	308
5.45	0.339	3.13	1.54	1.92	1.020	1.034	8.48	1.56	151	289
3.25	0.149	5.52	2.60	1.91	1.058	1.022	4.83	1.48	145	277
3.25	0.185	5.52	2.60	1.92	1.058	1.033	6.23	1.92	186	356
							av	1.77	172	330

[a] $\Gamma_{1,\text{eff}}$ and $\Gamma_{2,\text{eff}}$ are taken from time-resolved measurements of fluorescence decay rates following pulsed excitation.
[b] $\alpha \equiv 2e^{-17.2/0.695T}$.
[c] β_1 and β_2 are from the discussion following Eq. (6) with Γ_{br} from Ref. 5.
[d] $\bar{v}$ is the mean relative velocity of the atoms in the vapor.
[e] R_{21} is from Eq. (6).
[f] $k_{21} = R_{21}/n$.
[g] $\sigma_{21} = R_{21}/(n\bar{v})$.
[h] $\sigma_{12} = \alpha\sigma_{21}$ from detailed balance.

Comparing (13) and (14) we may formally define a Γ for the quasistatic regime,

$$\Gamma_{qs} \equiv \frac{4\pi^2}{3} C_3 n \ . \tag{15}$$

The two regimes are roughly separated by the critical detuning, $1/\tau_c \sim \bar{v}^{3/2}/C_3^{1/2} \sim 30$ GHz for the sodium D lines.[18,36] Here $\bar{v}$ is the mean relative velocity of atoms in the vapor.

Absorption coefficients in the collision-dominated limit ($\Gamma_{br} \gg \Gamma_N$) calculated by Movre and Pichler[17] using a quasistatic approximation and from Eq. (13) using the Carrington *et al.*[5] impact-regime Γ_{br}'s (where we have added the contributions from the two fine-structure levels incoherently) are plotted in Fig. 7. Also plotted are our measured absorption coefficients for $[Na] = 1.51 \times 10^{14}$ cm^{-3}. The asymmetry between the two wings of each line, beyond about 50 GHz, which is apparent in both the data and the Movre and Pichler calculations, is due to fine-structure recoupling and resultant curvature of the potential curves originating in the two fine-structure levels (see Ref. 17). The satellites in these calculations, at ~ 50 GHz in Fig. 7, are due to extrema in two of the potential curves. We do not observe these satellites and in fact see a much gentler onset of asymmetry than the calculations indicate. However, as expected and noted by Movre and Pichler, the satellites should be severely washed out in the lighter alkali-metals such as sodium due to a breakdown of the quasistatic approximation.

Niemax and Pichler[3] and Niemax, Movre, and Pichler[14] have studied quasistatic line shapes for self-broadened sodium, potassium, rubidium, and cesium. They observed asymmetries in all cases and broad satellites on the inner wings of the rubidium and cesium resonance doublets. Awan and Lewis[37] observed the same broad satellites in the case of rubidium. Our results for the line shape are in good agreement with those of Niemax and Pichler for Na.

VII. RESULTS FOR σ_{21}

The excitation-transfer cross sections were obtained from measurements of I_{D_1}/I_{D_2}. In these measurements, we tuned the cw laser well off resonance to obtain a uniform excitation along the laser column and to allow spectral resolution of the Rayleigh and fluorescence components. The beam diameter and detection height were both chosen to be 5 mm in an attempt to primarily fill and detect the fundamental excitation mode (see Refs. 18, 22, and 38). We measured the fluorescence ratio at several sodium densities and took $\Gamma_{1,\text{eff}}$ and $\Gamma_{2,\text{eff}}$ from time-resolved measurements of decay rates following pulsed excitation (see Refs. 18 and 22). Table II lists

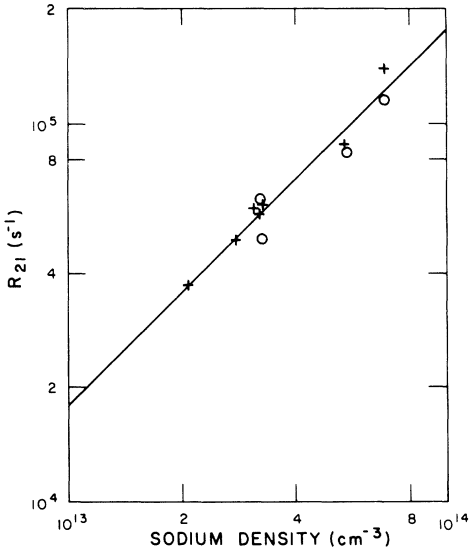

FIG. 8. R_{21} vs sodium density.

values of R_{21} determined from Eqs. (6a) and (6b) and the measured fluorescence ratios. Note that the factors β_i differ from unity by less than $\sim 5\%$ at our lowest densities and by less than 1% at our higher densities. Figure 8 is a plot of these values of R_{21} versus sodium density. These rates are turned into cross sections by the relationship $\sigma_{21} \equiv R_{21}/(n\bar{v})$, where $\bar{v}$ is the mean relative velocity of the colliding atoms. We thus obtain the average value for the cross section (of $\pm 18\%$ accuracy),

$$\sigma_{21} = 172 \text{ Å}^2 \ , \tag{16a}$$

and σ_{12} is obtained from detailed balance,

$$\sigma_{12} = 330 \text{ Å}^2 \ . \tag{16b}$$

The uncertainties come from the discussion which follows.

Measurements at higher densities than those listed in Table II were also made, but for $R_{21} > \Gamma_{2,\text{eff}}$ we get almost complete mixing, and the fluorescence ratio is very insensitive to the values of R_{21}. Additionally, the fluorescence ratio is very sensitive to $\Gamma_{1,\text{eff}}/\Gamma_{2,\text{eff}}$ which is least well known in the transition from the density range where trapping is dominated by Doppler broadening to that dominated by impact broadening (i.e., 6×10^{13} to 1×10^{14} cm^{-3}—see Refs. 18 and 22). Consequently, large uncertainties appear in data taken above 6×10^{13} cm^{-3}.

Note that Eqs. (4)—(6) do not contain the angular factors F_i, such as those appearing in the fluorescence to Rayleigh ratio used to obtain the resonance-broadening parameter [Eq. (8)]. This is because the D_1 and D_2 fluorescences, have the same angular factors as long as $k_0 L \gg 1$ for both lines.

According to Holstein's theory[28] of radiation trapping, the excited-atom spatial distribution as a function of time can be expanded in eigenmodes as

$$n_e(\vec{r},t)=\sum_i c_i n_i(\vec{r})e^{-\gamma_i t}. \quad (17)$$

The slowest decaying eigenvalue γ_1 is called the fundamental-mode decay rate Γ_{eff}.

In a pulsed experiment, higher modes decay more rapidly than the fundamental mode, so that a late time measurement of the decay rate is, in fact, a measurement of the fundamental-mode decay rate. However, in a cw experiment such as this, the presence of higher modes can be a serious source of systematic error since, in this case, the higher modes do not decay away. We have attempted to minimize the effects of higher modes by selecting the spatial dependence of the beam to correspond, as closely as possible, to the fundamental mode. We have used a laser beam diameter of ~ 5 mm (see Fig. 4) in order to fill $\sim 80\%$ of the window gap and thereby maximize the overlap of the beam with this fundamental-mode excited-atom spatial distribution (see Refs. 28 and 39).[40] We detect fluorescence from the 5-mm high region between the dashed lines in Fig. 4.

We can get an idea of the uncertainties in our cross-section results, Eq. (16), due to contributions of higher diffusion modes by measuring the change in the D_1 to D_2 fluorescence ratio as either the beam diameter or detection region height is changed (see Fig. 4). We made such measurements at $n=7.14\times10^{13}$ cm^{-3} with the laser frequency detuned ~ 31 GHz to the red of the D_2 line. The results of the measurements are presented in Fig. 9. As can be seen, the D_1 to D_2 fluorescence ratio changes by $\sim 10\%$ for extreme variations of beam diameter and detection height (a 10% change in I_{D_1}/I_{D_2} yields about a 20% change in σ_{21} at this density). We conclude that the presence of higher modes can contribute no more than $\sim 10\%$ uncertainty to our cross sections.

The uncertainty in our density measurements is of the order of 10%, while statistical uncertainty of the average cross section is $<5\%$ due to the large number of measurements made at many densities and detunings. Use of Holstein's theory for the ratio of $\Gamma_{1,\text{eff}}$ to $\Gamma_{2,\text{eff}}$ introduces an uncertainty of $\sim 10\%$. The uncertainty in $\Gamma_{2,\text{eff}}$ itself is relatively small (on the order of 5%) due to its derivation from measurements of the slow fluorescence decay rates following pulsed excitation. From these estimated uncertainties we assign our cross sections given in Eq. (16) an accuracy of $\pm 18\%$.

We also measured the excitation-transfer rate R_{21} using pulsed N_2-laser pumped dye laser excitation of the D_2 line and time-resolving the D_1 fluorescence signal using a fast transient digitizer.[18,22] In those references we show that the fast exponential buildup rate ω_+ of the D_1 fluorescence depends strongly on R_{21} at high densities, so that the measurements of ω_+ yield a value of $R_{21}/n=1.67\times10^{-9}$ cm^3/s with $\sim 20\%$ uncertainty. This translates into a cross section $\sigma_{21}=160$ Å^2 which is well within the combined uncertainties of our two measurements. Thus the pulsed measurement provides an independent confirmation of the cw results.

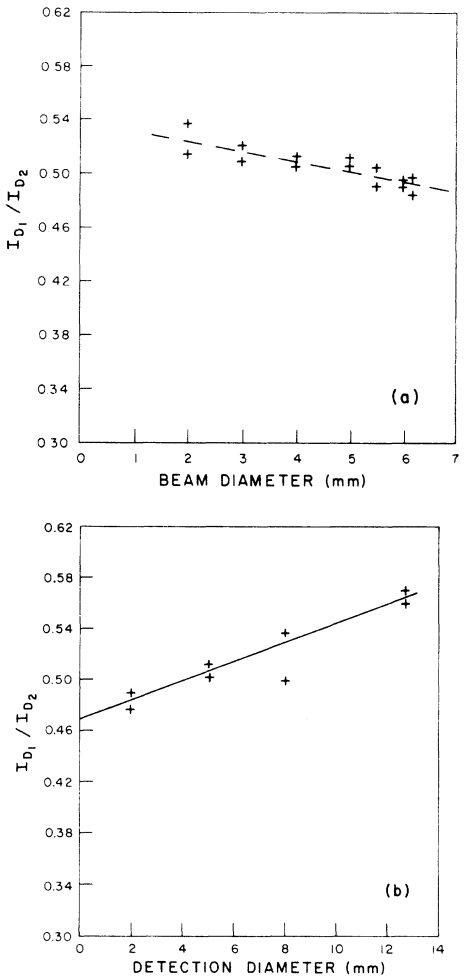

FIG. 9. (a) Ratio of the D_1 to D_2 fluorescence as a function of beam diameter, and (b) ratio of the D_1 to D_2 fluorescence as a function of detected region height in the vertical dimension (y). In both cases laser was detuned ~ 31 GHz to the red of the D_2 line. [Na]$=7.14\times10^{13}$ cm^{-3}. See Fig. 4 for geometry.

VIII. DISCUSSION OF RESONANCE BROADENING

Very few measurements of alkali-metal resonance broadening have been made, particularly in the im-

TABLE III. Comparison of experimental and theoretical determinations of the sodium resonance-broadening parameters $k_{br,2}$ for the D_2 line and $k_{br,1}$ for the D_1 line.

Author	$k_{br,2}$ (10^{-7} cm^3/s)	$k_{br,1}$ (10^{-7} cm^3/s)	$k_{br,2}/k_{br,1}$	Analytic Expression
		Experimental		
This work	4.67 (±15%)	3.07 (±15%)	1.52 (±10%)	
Niemax and Pichler[a]	6.84 [±(30−50)%]	5.79 [±(30−50)%]	1.18 [±(30−50)%]	
Watanabe[b]	5.85 (±20%)	5.04 (±20%)	1.16	
Popov and Ruzov[c]		3.88		
		Theoretical		
				$(D_2)2\pi\times 1.47e^2f/m\omega$
Carrington, Stacey and Cooper[d]	4.79	2.94	1.63	$(D_1)2\pi\times 1.805e^2f/m\omega$
				$2\pi\times 1.92(g/g^*)^{1/2}e^2f/m\omega$
Ali and Griem[e]	4.42	3.13	1.41	$(D_2)2\pi\times 1.61e^2f/m\omega$
Reck *et al.*[f]	5.25	3.42	1.54	$(D_1)2\pi\times 2.10e^2f/m\omega$

[a]Reference 3. [d]Reference 5.
[b]Reference 41. [e]Reference 4.
[c]Reference 42. [f]References 43 and 44.

pact regime. As seen in Sec. VI, the resonance interaction produces a Lorentzian line shape in both the quasistatic and impact limits, but the multiplicative constant is not necessarily the same in both regimes. A comparison of the Carrington, Stacey, and Cooper[5] impact-regime calculations and the Movre and Pichler[17] quasistatic calculations show that k_v(impact) and k_v(quasistatic) differ by ~ 5–40% in the detuning region where we took data (see Fig. 7). An expansion of the two-level Fourier integral theory indicates that near $\Delta\omega \sim 1/\tau_c$ the quasistatic approximation yields results that are $\sim 10\%$ too high.[36] On the other hand the first-order correction to the impact-limit result is proportional to $\Delta\omega$, and this correction is included in our linear interpolations to zero detuning (see Fig. 6) so that we are justified in reporting impact-regime results for k_{br}.

Niemax and Pichler[3] and Niemax, Movre, and Pichler[14] made measurements of the self-broadened wing absorption coefficients for sodium, potassium, rubidium, and cesium. From these k_v and Eq. (14) they determined C_3 coefficients, which we have converted to k_{br} coefficients using Eq. (15). Their values of k_{br} in sodium are listed in Table III along with an early measurement by Watanabe,[41] a measurement on the D_1 line by Popov and Ruzov,[42] and our results. Additionally, we list the theoretical values of k_{br} obtained by Carrington, Stacey, and Cooper[5] along with those obtained from two earlier calculations. The systematic discrepancy between our results and those of Niemax and Pichler falls within their estimated uncertainties but suggests a systematic effect in their density determination. Our results are in excellent agreement with the Carrington, Stacey, and Cooper and the Ali and Griem calculations. Our ±15% uncertainties are not, however, small enough to distinguish between the available theoretical results.

It should be noted that for $J=0$ to 1 transitions, the experimental results for k_{br} of Vaughan,[6] and Kuhn and Lewis[7] (He), Stacey and Thompson[8] (Ne), Lagarde and Lennuier[45] (Hg), and Penkin and Shabanove[46] (Ca, Sr, and Ba) are all in agreement with the results of Carrington *et al.*[5] as well as with those of other detailed models such as Berman and Lamb,[47] Omont and Meunier,[10] and Ali and Griem.[4] Additionally, Happer and Salomon[12] (Pb) and Omont and Meunier[10] (Hg) obtained results for collisional rates of destruction of orientation which are in agreement with these calculations. Gallagher and Lewis[11,16] (^{87}Rb perturbed by ^{85}Rb) obtained results for collisional rates of destruction of orientation in $J=\frac{1}{2}$ to $\frac{1}{2}$ and $J=\frac{1}{2}$ to $\frac{3}{2}$ transitions which agree with the Carrington, Stacey, and Cooper calculations to within experimental uncertainties of 6%. However, Hsieh and Baird's[48] results in thallium

disagreed with the theory by slightly more than the estimated uncertainties. The measurements of C_3 coefficients in cesium and rubidium made by Niemax *et al.*[14] have uncertainties of $\sim 30\%$ and are in good agreement with the calculations. Finally, Lewis *et al.*[9] obtained values for $k_{\rm br}$ in potassium, using the resonance state as the lower level, that are $\sim 30\%$ above the Carrington, Stacey, and Cooper, and Ali and Griem calculations but are uncertain by the same amount. A review article by Lewis[16] contains a summary of much of the work which has been carried out on the resonance interaction. Table 1 in Ref. 3, and Tables 1 and 2 in Ref. 14 compare resonance-broadening data taken in the quasistatic wings of all the alkali-metals. We believe that the present work is the most definitive confirmation of the most detailed calculations of $k_{\rm br}$ for $J=\frac{1}{2}$ to $\frac{1}{2}$ and $J=\frac{1}{2}$ to $\frac{3}{2}$ transitions.

Finally, we note that our result for the ratio $k_{\rm br,2}/k_{\rm br,1}$, which is independent of radiation-trapping corrections such as $F_{\rm fl}$ and the density determination, is 1.52 ($\pm 10\%$). This is also in good agreement with the calculations, as well as with the Lewis *et al.*[9] measurements in potassium and the Niemax *et al.*[14] measurements in cesium and rubidium.

IX. DISCUSSION OF EXCITATION TRANSFER

We are aware of two previous measurements of the excitation-transfer cross section σ_{21}. The first was by Seiwert[1] who obtained $\sigma_{21}=100$ Å^2. His measurements were made at high optical depth and used a resonance lamp as the excitation source. The data reduction required detailed calculations of the source intensity and spectral profile as functions of depth into the vapor, and similar calculations for the escaping fluorescence. It is remarkable that Seiwert's results agree as well as they do with later results considering the difficulty of these calculations and the sensitivity to the lamp profile. The second measurement of σ_{21} was by Pitre and Krause,[2] who obtained $\sigma_{21}=283$ Å^2. Their experiment was done under optically thin conditions, which avoids radiation-trapping problems. In this limit the fluorescence ratio reduces to $I_{D_1}/I_{D_2}\sim R_{21}/\Gamma_N$. Since Γ_N is well known, this is, in principle, a simple, accurate method for determining the excitation-transfer cross section. The major source of uncertainty in Pitre and Krause's work, however, has to be the determination of density from a vapor-pressure curve. Densities obtained in this way can be very inaccurate depending on temperature homogeneity and accuracy, surface contamination by background gas, reactions with window material, and the accuracy of the vapor-pressure relation itself in the relevant density region. A low optical-depth measurement also suffers from very weak sensitized fluorescence signals (on the order of 10^{-6} of the direct fluorescence signals) which increases statistical uncertainties and requires accurate calibration of the detection system (including neutral density filters) over a large range. Finally, when the D_2 line is being pumped, as in Pitre and Krause's experiment, the use of an anisotropic and polarized excitation source leads to partially polarized and therefore anisotropic D_2 fluorescence at low optical depths, but to unpolarized and isotropic D_1 fluorescence. This problem was mentioned by Pitre and Krause but was not quantitatively taken into account. Thus, despite their claim of 10% accuracy, we believe the actual uncertainty was much greater.

Calculations of the excitation-transfer cross sections for alkali-metals colliding with identical atoms are generally in poor agreement with the experimental results. In the case of sodium, Dashevskaya, Voronin, and Nikitin[49] obtained the value of $\sigma_{21}=101$ Å^2 from a calculation based on an assumption of an atomic interaction with a dipole-dipole long-range character. This is not too far from our experimental result of 172 Å^2, but their results for the other alkali-metals often disagree with experiment by more than an order of magnitude. Vdovin, Galitskii, and Dobrodeev[50] obtained $\sigma_{21}=131$ Å^2 for sodium in a calculation that neglected exchange effects. It is expected that better agreement between theory and experiment will be obtained when the more accurate molecular potential curves of Movre and Pichler[17] are employed in these calculations.

These theoretical and experimental results are presented in Table IV. A review article by Krause[51] tabulates results for fine-structure level changing collisions for all the alkali-metals interacting with atoms of the same and other species.

X. CONCLUSIONS

We have made accurate measurements of the sodium D_1- and D_2-line resonance-broadening parameters. These measurements have confirmed, within experimental uncertainties of $\pm 15\%$, the accuracy of the more complete resonance-broadening calculations for $J=\frac{1}{2}$ to $\frac{1}{2}$ and $J=\frac{1}{2}$ to $\frac{3}{2}$ transitions (see Table III). The resonance-broadening measurements we made are significant for several reasons. (1) They confirm, within 15%, the present impact theories of resonance broadening, even though these theories do not consider the fine-structure recoupling. (2) Confirmation of the resonance-broadening calculations for sodium offers

TABLE IV. Experimental and theoretical cross sections for excitation transfer in Na-Na collisions.

Authors	$\sigma_{21}(\mathrm{Na}(3S)+\mathrm{Na}(3P_{3/2}) \rightarrow \mathrm{Na}(3S)+\mathrm{Na}(3P_{1/2}))$ (Å^2)	$\sigma_{12}(\mathrm{Na}(3S)+\mathrm{Na}(3P_{1/2}) \rightarrow \mathrm{Na}(3S)+\mathrm{Na}(3P_{3/2}))$ (Å^2)	Temperature (K)
	Experiment		
This work	172 (±18%)	330 (±18%)	575
Pitre and Krause[a]	283	532	424
Seiwert[b]	100	170	560
	Theory		
Dashevskaya *et al.*[c]	101		
Vdovin *et al.*[d]	131	229	

[a]Reference 2.
[b]Reference 1.
[c]Reference 49.
[d]Reference 50.

researchers a fairly accurate method of determining the sodium vapor density simply by measuring the wing absorption coefficient. The same procedure can probably be safely extended to the other alkali-metals as well. (3) These broadening parameters can be used with confidence to within ±15% by anyone working at high optical depth who uses Holstein's[28] theory to calculate radiation-trapping effects in their experiment.

We have studied the collisional part of the D_1- and D_2-line absorption coefficients as a function of detuning. The line shapes which we obtained for the resonance doublet, in the detuning range 20—150 GHz, show approximately Lorentzian outer wings (blue for D_2, red for D_1) but inner wings that fall below the outer wings for detunings greater than ~50 GHz (see Fig. 7). This behavior was theoretically predicted by Movre and Pichler[17] whose calculations yield a satellite at ~50 GHz on the inner wing followed by asymmetry beyond the satellite (see Fig. 7). Our results for the line shape are consistent with this theory and with the measurements of Niemax and Pichler.[3]

Finally, we have made measurements of the effective radiative decay rates of the resonance lines in the presence of radiation trapping, as a function of density, using pulsed excitation and time-resolved detection of fluorescence. The measured values of the Γ_{eff}'s were then used in connection with cw measurements of the D_1 to D_2 fluorescence ratio, when either line was excited, to obtain improved values for the $3P_{3/2}$-$3P_{1/2}$ excitation-transfer cross sections [Eqs. (16a) and (16b)].

ACKNOWLEDGMENTS

We would like to thank Dr. Jinx Cooper and Dr. Keith Burnett for many enlightening discussions during the course of this work. We would also like to thank Dr. Wolfgang Kamke for much assistance in the operation of the laser. This work was supported in part by National Science Foundation Grant No. PHY-79-04928 through the University of Colorado.

*Present address: Physics Department, Princeton University, Princeton, NJ 08544.
†Quantum Physics Division, National Bureau of Standards.

[1]R. Seiwert, Ann. Phys. (Leipzig) 18, 54 (1956).
[2]J. Pitre and L. Krause, Can. J. Phys. 46, 125 (1968).
[3]K. Niemax and G. Pichler, J. Phys. B 8, 179 (1975).
[4]A. W. Ali and H. R. Griem, Phys. Rev. 140, A1044 (1965); 144, A366 (1966).
[5]C. G. Carrington, D. N. Stacey, and J. Cooper, J. Phys. B 6, 417 (1973).
[6]J. M. Vaughan, Proc. R. Soc. London, Ser. A 295, 164 (1966).
[7]H. G. Kuhn and E. L. Lewis, Proc. R. Soc. London, Ser. A 299, 423 (1967).
[8]D. N. Stacey and R. C. Thompson, Acta Phys. Pol. A 54, 833 (1978).
[9]E. L. Lewis, M. M. Rebbeck, and J. M. Vaughan, J. Phys. B 741 (1971).
[10]A. Omont and J. Meunier, Phys. Rev. 169, 92 (1968).
[11]A. Gallagher and E. L. Lewis, Phys. Rev. A 10, 231 (1974); 16, 1337 (1977).
[12]W. Happer and E. B. Saloman, Phys. Rev. 160, 23 (1967).
[13]C. L. Chen and A. V. Phelps, Phys. Rev. 173, 62 (1968).
[14]K. Niemax, M. Movre, and G. Pichler, J. Phys. B 12, 3503 (1979).

[15]J. Holtsmark, Z. Phys. 34, 722 (1925).
[16]E. L. Lewis, Phys. Rep. 58, 1 (1980).
[17]M. Movre and G. Pichler, J. Phys. B 10, 2631 (1977); 13, 697 (1980).
[18]J. P. Huennekens, Ph.D. thesis, University of Colorado, 1982 (unpublished).
[19]We would like to thank David Pritchard and Derek Robb for useful discussions concerning these terms. See also the article by D. E. Pritchard and R. E. Walkup, in Proceedings of the Sixth International Conference on Spectral Line Shapes, edited by K. Burnett (de Gruyter, New York, in press).
[20]S. Reynaud and C. Cohen-Tannoudji, in *Laser Spectroscopy V*, edited by A. R. W. McKellar, T. Oka, and B. P. Stoicheff (Springer, Berlin, 1981), p. 166.
[21]K. Burnett, J. Cooper, P. D. Kleiber, and A. Ben-Reuven, Phys. Rev. A 25, 1345 (1982).
[22]J. Huennekens and A. Gallagher, Phys. Rev. A (in press).
[23]A. N. Nesmeyanov, *Vapor Pressure of the Elements* (Academic, New York, 1963).
[24]R. Loudon, *The Quantum Theory of Light* (Clarendon, New York, 1973).
[25]E. U. Condon and G. H. Shortley, *The Theory of Atomic Spectra* (Cambridge University Press, Cambridge, 1935).
[26]R. J. Ballagh and J. Cooper, Astrophys. J. 213, 479 (1977).
[27]A. C. Tam and C. K. Au, Opt. Commun. 19, 265 (1976).
[28]T. Holstein, Phys. Rev. 72, 1212 (1947); 83, 1159 (1951).
[29]C. V. Kunasz and P. B. Kunasz, Comput. Phys. Commun. 10, 304 (1975).
[30]L. H. Aller, *Astrophysics—The Atmospheres of the Sun and Stars* (Ronald, New York, 1953).
[31]L. K. Lam, T. Fujimoto, and A. C. Gallagher, J. Chem. Phys. 68, 3553 (1978).
[32]A. Corney, *Atomic and Laser Spectroscopy* (Clarendon, Oxford, 1977).
[33]A. C. G. Mitchell and M. W. Zemansky, *Resonance Radiation and Excited Atoms* (Cambridge University Press, Cambridge, 1934).
[34]K. Niemax and G. Pichler, J. Phys. B 7, 1204 (1974).
[35]A. V. Phelps, Joint Institute for Laboratory Astrophysics Report No. 110, University of Colorado, Boulder, Colo., 1972 (unpublished).
[36]T. Holstein, Phys. Rev. 79, 744 (1950).
[37]M. S. Awan and E. L. Lewis, J. Phys. B 9, L551 (1976).
[38]J. Huennekens and A. Gallagher Phys. Rev. A 27, 771 (1983).
[39]C. van Trigt, Phys. Rev. 181, 97 (1969).
[40]Figures 1–5 of Ref. 39 give an idea of the dependences on x of the excited-atom spatial distributions of the first few eigenmodes in an infinite slab. (van Trigt's calculations are based on Holstein's theory incorporating some minor improvements. The results, however, agree well with those obtained by Holstein.)
[41]K. Watanabe, Phys. Rev. 59, 151 (1941).
[42]K. G. Popov and V. P. Ruzov, Opt. Spektrosk. 48, 675 (1980) [Opt. Spectrosc. (U.S.S.R.) 48, 372 (1980)].
[43]G. P. Reck, H. Takebe, and C. A. Mead, Phys. Rev. 137, A683 (1965).
[44]C. A. Mead, Int. J. Theor. Phys. 1, 17 (1968).
[45]D. Legarde and R. Lennuier, C. R. Acad. Sci. 261, 919 (1965).
[46]N. P. Penkin and L. M. Shabanova, Opt. Spektrosk. 26, 346 (1969) [Opt. Spectrosc. (U.S.S.R.) 26, 191 (1969)].
[47]P. R. Berman and W. E. Lamb, Phys. Rev. 187, 221 (1969).
[48]J. C. Hsieh and J. C. Baird, Phys. Rev. A 6, 141 (1972).
[49]E. I. Dashevskaya, A. I. Voronin, and E. E. Nikitin, Can. J. Phys. 47, 1237 (1969).
[50]Yu. A. Vdovin, V. M. Galitskii, and N. A. Dobrodeev, Zh. Eksp. Teor. Fiz. 56, 1344 (1969) [Sov. Phys.—JETP 29, 722 (1969)].
[51]L. Krause, in *The Excited State in Chemical Physics*, edited by J. W. McGowan (Wiley, New York, 1975), pp. 267–316.